

Influence of melt temperature on the compressive plasticity of a Zr–Cu–Ni–Al–Nb bulk metallic glass

Xie-rong Zeng · Sheng-hui Xie · Qiang Hu ·
Dong-ju Fu · Hai-xia Qian · Ming-wang Fu

Received: 25 May 2010/Accepted: 14 August 2010/Published online: 8 September 2010
© Springer Science+Business Media, LLC 2010

Abstract $Zr_{63.78}Cu_{14.72}Ni_{10}Al_{10}Nb_{1.5}$ BMGs (bulk metallic glasses) were cast at the melt temperatures ranging from 1,073 to 1,313 K with the same interval of 40 K. The structure, thermal, and mechanical properties of the BMGs were investigated by XRD, DSC, HRTEM, dilatometric measurements, micro-hardness tests, and uniaxial compression. The results indicate that the higher the casting temperature, the fewer the nano-crystallites, the more the free volumes, and the lower the micro-hardness in the BMGs, leading to the larger plastic strains. The plasticity of BMGs deteriorates with the increase of nano-crystallites as decreasing the casting temperature. The free volume, instead of the nano-crystallites, favors the plastic deformation in $Zr_{63.78}Cu_{14.72}Ni_{10}Al_{10}Nb_{1.5}$ BMGs. The microstructures and mechanical performance of BMGs are closely affected by the casting temperature. The preparing parameters are important to improve the plasticity of the BMGs.

Introduction

In the last three decades, bulk metallic glasses (BMGs) have attracted considerable attention due to their unique physical, mechanical, and chemical properties [1–4]. Many BMGs have also been developed in many alloy systems free of noble metals, such as Zr-, Fe-, Mg-, Cu-, and Ti-based alloys. Many researchers have been exerting themselves to develop new BMG-forming systems with good glass-forming ability and study the corresponding physical, chemical, mechanical, and oxidation behavior of these new BMG alloys, aiming at the engineering application of the new materials [5–7]. Especially, the plastic deformation behavior of BMGs has attracted wide research because they can be deployed in structural applications, as they exhibit extraordinary strength and large elastic limit [1–5, 8]. However, unlike conventional metal in which the atoms are arranged in orderly arrays, the atomic arrangements in BMGs have just short-range but no long-range order. Thus, the deformation mechanism of BMGs is fundamentally different from their crystalline counterparts. The BMGs lack the typical deformation mechanisms, such as dislocation slip, glide, and twinning based on the lattice theory. Therefore, most BMGs that have been reported exhibit little macroscopic plasticity at room temperature [9, 10]. It is widely recognized that the microstructure of BMGs plays a significant role in affecting their mechanical performance in spite of the unclear deformation mechanisms. It has also been confirmed by many researchers that the plasticity in BMGs can largely be enhanced by introducing interior heterogeneities (nano-crystalline, nano-quasicrystalline, phase separation, free volume, in situ dendrite, etc.) into BMGs, which can facilitate the initiation, bifurcation, and intersection of shear bands [11–20]. However, some researchers also witnessed the

X. Zeng (✉) · S. Xie · Q. Hu · D. Fu
School of Materials Science and Engineering,
Northwestern Polytechnical University, Xi'an 710072, China
e-mail: zengxierong@163.com

X. Zeng · H. Qian
College of Materials Science and Engineering,
Shenzhen University, Shenzhen, China

X. Zeng · H. Qian
Shenzhen Key Laboratory of Special Functional Materials,
Shenzhen 518060, China

M. Fu
Department of Mechanical Engineering, The Hong Kong
Polytechnic University, Hong Kong, China

unfavorable effect of nano-crystal on plastic deformation in BMGs [21–23]. The deformation-induced structural evolution also has distinct influence on the mechanical properties and plastic deformation in BMGs [24–26]. Therefore, the influence of microstructure of BMGs on the plasticity is still elusive and needs further investigation. Usually, the microstructure of BMGs is closely related to the preparation methods, especially the casting conditions [27]. The BMGs can inherit some structural information from their melt states, while the melt structure can largely be regulated by the temperature [28–32]. Therefore, the melt temperature (casting temperature) should have distinct impacts on the microstructures of BMGs and their deformation behavior. Some researchers have found that the solidification conditions have obvious impact on the plasticity in three BMGs systems [27]. However, the detailed information regarding the influence of melt temperature on the structure and mechanical performance of BMGs is not available.

In this article, we will explore the relationship in detail between the melt temperature and the microstructures or the mechanical performance of BMGs. $Zr_{63.78}Cu_{14.72}Ni_{10}Al_{10}Nb_{1.5}$ BMG-forming alloy is selected in this study because it consists of only inexpensive elements and possesses good plasticity at room temperature. It is found that the change in the melt temperature has distinct impact on the plastic deformation in BMGs. Excessive precipitation of nano-crystals can deteriorate the plasticity of BMGs. This article suggests a practical way to control the microstructure or the plasticity of BMGs by regulating the casting temperature (melt temperature).

Experimental details

The $Zr_{63.78}Cu_{14.72}Ni_{10}Al_{10}Nb_{1.5}$ master alloys were prepared using arc melting the mixtures of the pure elements (>99.9%) with the appropriate ratios of Zr, Cu, Ni, Al, and Zr–Nb intermediate alloys which were arc-melted in advance, in the Ti-gettered argon atmosphere with 99.999% purity. The alloys were re-melted at least four times to ensure the compositional homogeneity. Finally, the cylindrical rods of 2 mm in diameter were cast by injecting the alloy melts at different temperatures (ranging from 1,033 to 1,313 K with the same interval of 40 K) into a copper mold under the argon atmosphere with 99.999% purity on a Rapid Quench Machine System (VF-RQT50). When the casting temperature is lower than 1,033 K, casting was difficult due to the high viscosity. When the casting temperature is higher than 1,313 K, obvious crystallization was observed in the as-cast rods. Therefore, the melt temperature for casting spans the whole range where the amorphous rods can be produced. The temperature

measurements were performed on a portable radiation thermometer (IR-AH, CHINO) with a fixed blackness coefficient of 0.75. The phase structures were investigated by X-ray diffraction (XRD) using a Bruker D8 Advance 18 kW X-ray diffractometer with $Cu\ K_\alpha$ radiation ($\lambda = 0.154178$ nm). The glass transition and the crystallization behavior were determined by the differential scanning calorimetry (DSC) using a Netzsch DSC 200 F3 under a continuous argon flow at the heating rate of 0.33 K s^{-1} . The quasi-static-compression tests were carried out on the cylindrical rods (2 mm in diameter and 4 mm in length) sandwiched between two tungsten carbide disks using a universal testing machine (Regr5500 Reger, China) with an initial strain rate of $5 \times 10^{-5}\text{ s}^{-1}$ at room temperature. The samples for the quasi-static-compression tests were cut from the long rods. The ends of the samples were polished to make them parallel to each other and perpendicular to the axis of the rod prior to compression tests using a carefully designed jig. The stress and the strain quantities presented here are the engineering stress and engineering strain data. The dilatometric measurements were conducted on a NETZSCH DIL 402C dilatometer with a resolution of $\Delta L = 1.25$ nm at the heating rate of 0.083 K s^{-1} under a compressive load of 0.3 N. The samples for dilatometric measurements are cylindrical rods with 2 mm in diameter and 25 mm in length. The micro-hardness measurements were performed using a Vickers hardness tester (HXD-1000TM/LCD) with 1.961 N loading and 10 s duration on the polished surfaces. The detailed microstructures were characterized with high resolution transmission electron microscope (HRTEM, JEOL 3010, 200KV). The thin foil specimens for HRTEM were prepared by ion beam miller (Gatan, Model 691) at 5 KeV and 5 mA. The ion beam milling was suspended for 10 min after every 15-min milling to avoid the potential temperature rise in the specimens.

Results and discussion

Figure 1 shows the XRD patterns of the as-cast $Zr_{63.78}Cu_{14.72}Ni_{10}Al_{10}Nb_{1.5}$ alloy rods with a diameter of 2 mm cast from the melt temperature range of 1,073–1,313 K. The patterns of all the rods consist of a single broad halo peak only with no detectable crystalline Bragg peaks, characteristic of the glassy structure. The DSC curves for all the as-cast $Zr_{63.78}Cu_{14.72}Ni_{10}Al_{10}Nb_{1.5}$ alloy rods prepared from different melt temperatures exhibit an endothermic event corresponding to the glass transition and a supercooled liquid region, followed by two exothermic events characteristic of the sequence of crystallization processes. The crystallization involves a two-step process, as shown in Fig. 2. The XRD and DSC

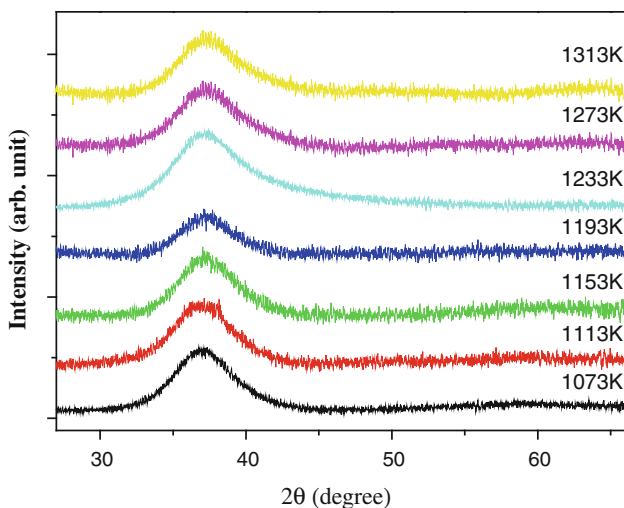


Fig. 1 X-ray diffraction patterns of $Zr_{63.78}Cu_{14.72}Ni_{10}Al_{10}Nb_{1.5}$ alloy rods cast at different temperatures

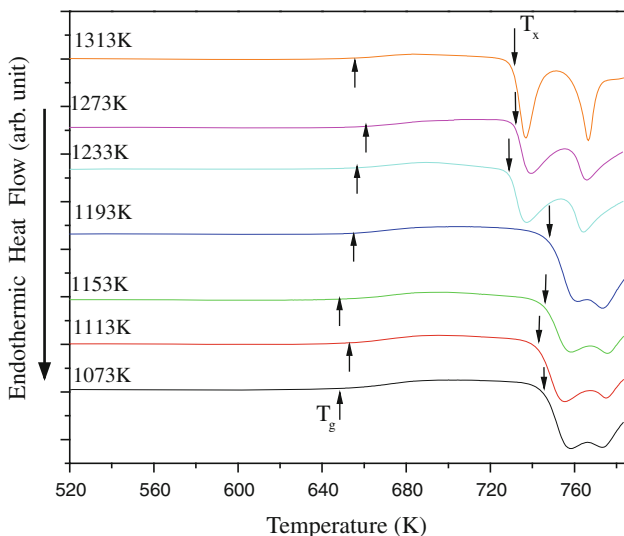


Fig. 2 DSC traces (heating rate of 0.33 K/s) of $Zr_{63.78}Cu_{14.72}Ni_{10}Al_{10}Nb_{1.5}$ alloy rods cast at different temperatures

results show the glassy nature of the as-cast alloys prepared from different melt temperatures within the experimental uncertainty of XRD and DSC.

Figure 3 shows the stress-strain curves of the $Zr_{63.78}Cu_{14.72}Ni_{10}Al_{10}Nb_{1.5}$ alloy rods cast from the melt temperatures in the range of 1,073–1,313 K. For each casting condition, five samples were cut from three different rods prepared in the same conditions for compression tests to ensure the reliability of the results. The typical stress-strain curves are shown in Fig. 3. The relationship between the average plastic strains and casting temperature for $Zr_{63.78}Cu_{14.72}Ni_{10}Al_{10}Nb_{1.5}$ BMGs is shown in Fig. 4. It can be concluded that the melt temperature (casting temperature) has distinct effect on the plasticity of

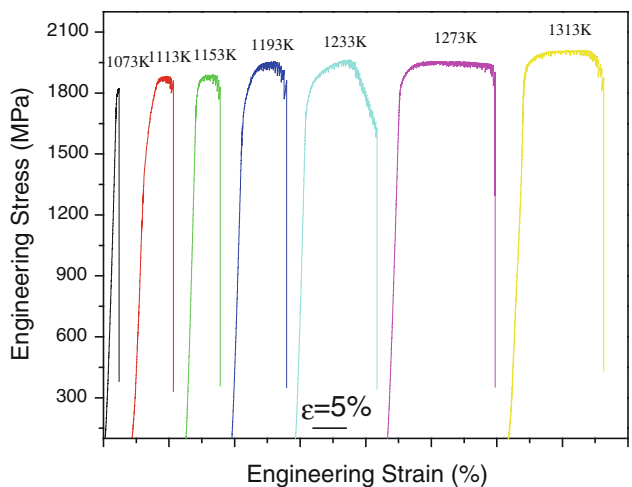


Fig. 3 The typical stress–strain curves of $Zr_{63.78}Cu_{14.72}Ni_{10}Al_{10}Nb_{1.5}$ alloy rods cast at different temperatures

$Zr_{63.78}Cu_{14.72}Ni_{10}Al_{10}Nb_{1.5}$ BMGs. The plastic strains of BMGs increase with increasing the melt temperature lower than 1,273 K, but decrease with further increasing the casting temperature. The maximum average plastic strain of 15.14% was found in the rods cast from 1,273 K, but no plastic strain was detected in the rods cast from 1,073 K. A question raised here is: How does the casting temperature result in such tremendous difference on the mechanical performance of BMGs?

In order to obtain more information on the structures of the BMGs cast from different temperatures, the dilatometric measurements and micro-hardness tests were performed on the samples. Figure 5 shows the corresponding linear thermal expansion vs temperature curves for the $Zr_{63.78}Cu_{14.72}Ni_{10}Al_{10}Nb_{1.5}$ BMGs cast at different temperatures from 1,073 and 1,313 K. The first heating cycle was up to 643 K, just below the glass transition temperature, and then holding at this temperature for 3,600 s that the samples sustained the sufficient structural relaxation. The second heating cycle was up to 873 K, higher than the crystallization temperature. The other curves are not shown here due to the similarity. The results show that the rods attain different relaxed excess free volumes (REFVs) after annealing just below T_g (as indicated by the double-head arrows in Fig. 5) for the BMGs cast from different temperatures. It should be noted that a non-linear relationship exists between the samples' temperature and time at the initial stage of heating (usually below 470 K) because of the lag between the samples' temperature and the furnace's temperature recorded by the non-contact temperature measurement in thermal dilatometer. Therefore, the reference point to calculate REFV is set as 473 K. Figure 6 shows the relationship between REFV and the casting temperature for $Zr_{63.78}Cu_{14.72}Ni_{10}Al_{10}Nb_{1.5}$ BMGs, indicating that REFV has the similar dependence on casting

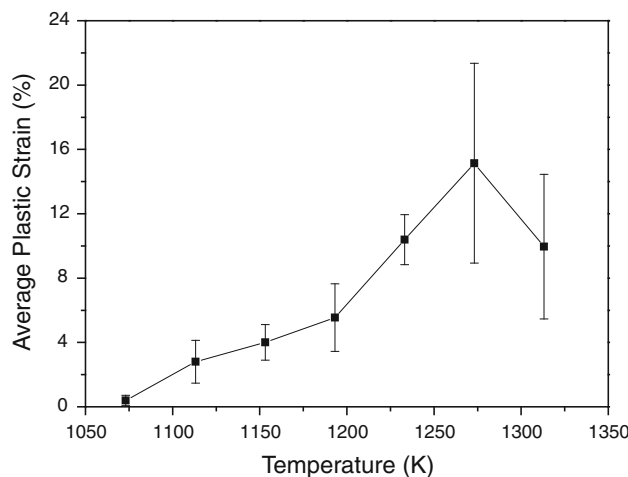


Fig. 4 The average plastic strain dependence of the casting temperature for $Zr_{63.78}Cu_{14.72}Ni_{10}Al_{10}Nb_{1.5}$ BMGs

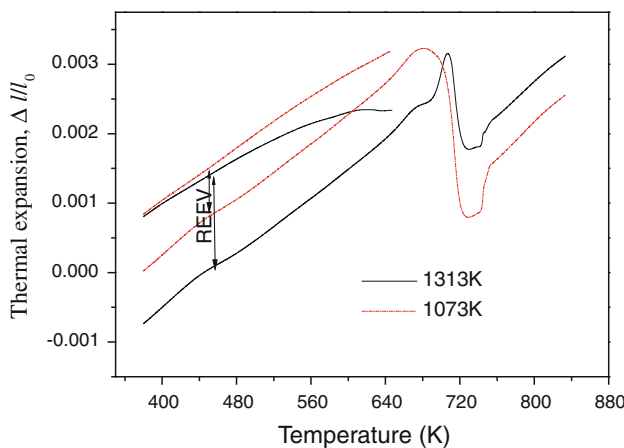


Fig. 5 The linear thermal expansion dependence of temperature for the $Zr_{63.78}Cu_{14.72}Ni_{10}Al_{10}Nb_{1.5}$ BMGs cast at 1,073 and 1,313 K (with heating rate of 0.0833 K s^{-1}). The first heating cycle was up to 643 K, just below the glass transition temperature, then holding for 3,600 s. The second heating cycle was up to 873 K, higher than the crystallization temperature. The holding zones are not visible here due to the temperature reference axis

temperature as the plasticity of BMGs has. It means that the more the REFVs that the BMGs have, the better the plasticity that they exhibit. This result coincides with that reported before [33]. The REFV after annealing just below T_g can quantificationally describe the amount of FV trapped in BMGs. The larger REFV value means more free volume being trapped in BMGs during casting. The free volume in BMGs acts as the site for the shear band initiation and branching. Therefore, it results in more plastic deformation in BMGs. Figure 6 also shows the relationship between micro-hardness and the casting temperature for $Zr_{63.78}Cu_{14.72}Ni_{10}Al_{10}Nb_{1.5}$ BMGs. It can be easily seen that the micro-hardness has an opposite relationship with casting temperature compared to that the plasticity and REFV of

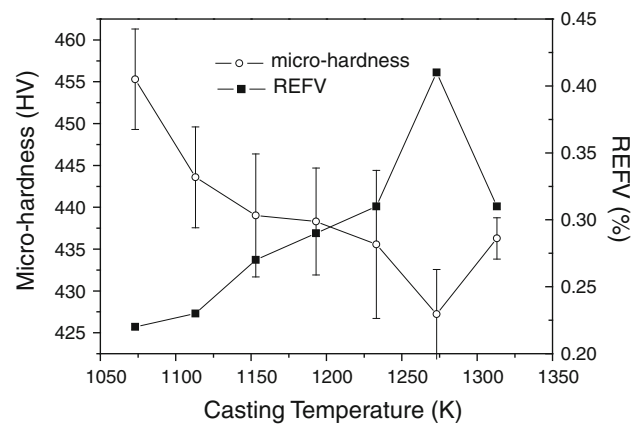


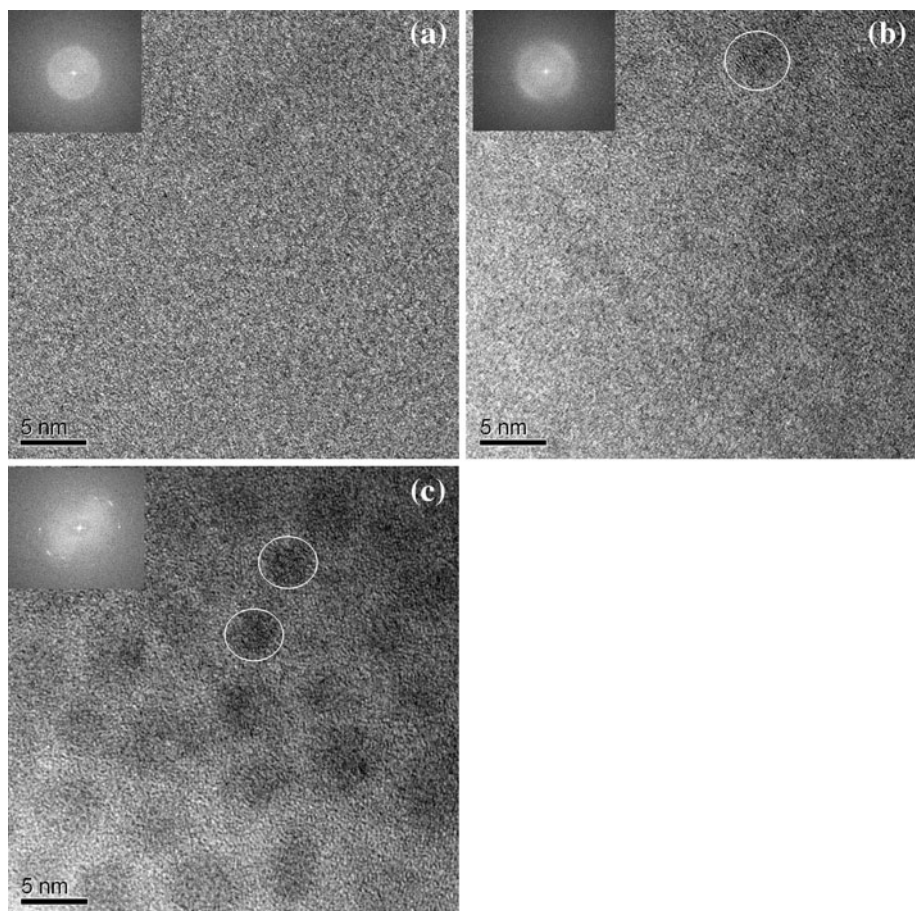
Fig. 6 The relationships of REFV and the micro-hardness with the casting temperature for $Zr_{63.78}Cu_{14.72}Ni_{10}Al_{10}Nb_{1.5}$ BMGs

BMGs have. The BMGs with more free volume trapped within would have the looser structure and the lower micro-hardness value. Then another question raised here is: How does the casting temperature result in such tremendous difference in the structure of BMGs (free volume content)?

In order to obtain the detailed structural discrepancy caused by the casting temperature, the samples were prepared for HRTEM observation. The results are shown in Fig. 7. As to the sample cast at 1,273 K, the HRTEM image (Fig. 7a) shows a homologous contrast indicating no obvious nucleation of crystallites. The Fourier transformation inset in Fig. 7a also shows the glassy nature of the sample. As regards the sample cast at 1,233 K, HRTEM image (Fig. 7b) shows a few crystal nuclei embedded in the amorphous matrix. There are about 10 layers of regular atomic arrangement among the crystal nuclei. The sample cast at 1,313 K also shows the same microstructure in the HRTEM image just as in Fig. 7b. However, the sample cast at 1,073 K has different microscopic features in the HRTEM images, as shown in Fig. 7c. It exhibits distinct lattice fringes of several nanometers, indicating that nano-crystallites are formed and are embedded in the glassy matrix. Due to the small size and small quantities, these nano-crystallites cannot be detected by XRD. The rest of the samples have some nano-crystallites, the amount of which falls between those of samples cast from 1,073 and 1,233 K.

Exploring the microstructure feathers of HRTEM images with other structural and mechanical results, the following consequence can be rationalized. The casting temperature 1,273 K ensures that the samples have the monolithic amorphous structure. The local structural-ordering clusters exist in the glass-forming melts for the lower temperature injection casting [28–32], which act as the nuclei during the solidification. In the higher-temperature injection casting, greater heat energy in the melts promotes the nucleation during the solidification.

Fig. 7 The HRTEM images of $Zr_{63.78}Cu_{14.72}Ni_{10}Al_{10}Nb_{1.5}$ BMGs cast at 1,273 K (a), 1,233 K (b), and 1,073 K (c) inset with the Fourier transformation taken from the same zones. Some nano-crystallites are marked by circles



Therefore, both higher and lower casting temperatures result in the precipitation of nano-crystallites. The samples embedded with no or a little amount of nano-crystallite (when casting temperature is higher than 1,193 K) exhibit relatively loose structures, larger amount of REFV, lower micro-hardness, and larger plastic strains. On further decreasing the casting temperature, the BMGs obtain more nano-crystallites precipitation, which depletes the free volume in BMGs and ensures that the BMGs have relatively more compact structures, less REFVs, higher micro-hardness, and smaller plastic strains. Apparently, these results are contradictory with that of Zhu [27], which indicates that the nano-crystallites have favorable influence on the plastic deformation by regulating the solidification condition for three Zr-based BMGs free of Nb. A reasonable explanation for this discrepancy may be due to the difference in alloying composition. The Nb addition changes the types and properties of primary crystals. Of course, how the types, amount, patterns and properties of nano-crystallites influence the plastic deformation still needs further in-depth investigation. In these experiments, $Zr_{63.78}Cu_{14.72}Ni_{10}Al_{10}Nb_{1.5}$ BMGs cast from the relatively higher temperature have larger amounts of free volume and the looser structure. The free volume trapped within BMGs

acts as the site for the shear band initiation and branching. Therefore, it results in large plasticity in BMGs. For the BMGs prepared at lower casting temperature, the plasticity deteriorates with the precipitation of nano-crystallites and the decrease of free volume. It is worthy to note that some researchers [34] have found improved plasticity in $Zr_{55}Cu_{30}Al_{10}Ni_5$ BMGs with low temperature annealing. Although the free volume in BMGs decreases upon annealing, the nanoscale inhomogeneities (Cu clusters) caused by the decomposition between Cu and Zr are believed to improve the plasticity in BMG. Various inhomogeneities including the nanoscale clusters and free volume all have significant influence on the improvement of plasticity of BMGs. All these evidences indicate that it is the free volume, not the nano-crystallites or other inhomogeneities, which is the decisive factor to favor the plastic deformation in $Zr_{63.78}Cu_{14.72}Ni_{10}Al_{10}Nb_{1.5}$ BMGs as indicated in this experiment.

Conclusions

To summarize, the $Zr_{63.78}Cu_{14.72}Ni_{10}Al_{10}Nb_{1.5}$ BMGs were fabricated by copper mold casting from melt temperatures

ranging from 1,033 to 1,313 K with the same interval of 40 K. The experimental results suggest that the different melt temperatures can cause different microstructures and plastic deformation behaviors. The higher the casting temperature is, the less the amount of nano-crystallites is and the more the free volumes are in the BMGs, resulting in the larger plastic strains for $Zr_{63.78}Cu_{14.72}Ni_{10}Al_{10}Nb_{1.5}$ BMGs. However, the lower the casting temperature is, the more the amount of nano-crystallites is and the less the free volumes are in the BMGs, resulting in the smaller plastic strains. The free volume, instead of the nano-crystallites, favors the plastic deformation in the $Zr_{63.78}Cu_{14.72}Ni_{10}Al_{10}Nb_{1.5}$ BMGs. The microstructures and mechanical performance of BMGs are severely affected by the casting temperature. The article has proposed a practical method to improve the plasticity in BMGs by regulating the preparing parameters.

Acknowledgements This research was supported by Shenzhen Science and Technology Research Grant (Grant No. CBX200903090012A), the Two Hundred Plan for Talent Station of Shenzhen (Shenfu [2008] No. 182), and the Open Project Program of Shenzhen Key Laboratory of Special Functional Materials (Grant No. T0907). The authors thank Lin Weichun and Luo Guangqin for their help in the experiments.

References

1. Inoue A (2000) *Acta Mater* 48:279
2. Ashby MF, Greer AL (2006) *Scr Mater* 54:321
3. Zhang L, Cheng YQ, Cao AJ et al (2009) *Acta Mater* 57:1154
4. Hays CC, Kim CP, Johnson WL (2001) *Mater Sci Eng A* 304–306:650
5. Wang WH, Dong C, Shek CH (2004) *Mater Sci Eng R* 44:45
6. Xu Y, Wang YL, Liu XJ et al (2009) *J Mater Sci* 44:3861. doi: [10.1007/s10853-009-3523-7](https://doi.org/10.1007/s10853-009-3523-7)
7. Sharma SK, Strunskus T, Ladebusch H et al (2008) *J Mater Sci* 43:5495. doi: [10.1007/s10853-008-2834-4](https://doi.org/10.1007/s10853-008-2834-4)
8. Greer AL (1995) *Science* 267:1947
9. Schuh CA, Hufnagel TC, Ramamurty U (2007) *Acta Mater* 55:4067
10. Johnson WL (1999) *MRS Bull* 24:42
11. Park ES, Kyeong JS, Kim DH (2007) *Scr Mater* 57:49
12. Kuhn U, Mattern N, Gebert A et al (2005) *J Appl Phys* 98:054307
13. Fan C, Qiao D, Wilson TW et al (2006) *Mater Sci Eng A* 431:158
14. Pan DG, Zhang HF, Wang AM et al (2006) *Appl Phys Lett* 89:261904
15. Mondal K, Ohkubo T, Toyama T et al (2008) *Acta Mater* 56:5329
16. Dong W, Zhang H, Cai J et al (2006) *J Alloys Compd* 425:L1
17. Kim KB, Das J, Baier F et al (2006) *Appl Phys Lett* 88:051911
18. Qiang JB, Zhang W, Xie GQ et al (2007) *Appl Phys Lett* 90:231907
19. Chen MW, Inoue A, Zhang W et al (2006) *Phys Rev Lett* 96:245502
20. Luo XM, Zhou Y, Lu JQ et al (2009) *J Mater Sci* 44:4389. doi: [10.1007/s10853-009-3661-y](https://doi.org/10.1007/s10853-009-3661-y)
21. Nagendra N, Ramamurty U, Goh TT et al (2000) *Acta Mater* 48:2603
22. Basu J, Nagendra N, Li Y et al (2003) *Phil Mag* 83:1747
23. Liang WZ, Mao XY, Wu LZ et al (2009) *J Mater Sci* 44:201. doi: [10.1007/s10853-009-3244-y](https://doi.org/10.1007/s10853-009-3244-y)
24. Lee MH, Lee KS, Das J et al (2010) *Scr Mater* 62:678
25. Tekaya A, Labdi S, Benameur T et al (2009) *J Mater Sci* 44:4930. doi: [10.1007/s10853-009-3752-9](https://doi.org/10.1007/s10853-009-3752-9)
26. Zhang PN, Li JF, Hu Y et al (2008) *J Mater Sci* 43:7179. doi: [10.1007/s10853-008-3019-x](https://doi.org/10.1007/s10853-008-3019-x)
27. Zhu ZW, Zheng SJ, Zhang HF et al (2008) *J Mater Res* 23:941
28. Busch R, Bakke E, Johnson WL (1998) *Acta Mater* 46:4725
29. Saboungi ML, Blomquist R, Volin KJ et al (1987) *J Chem Phys* 87:2278
30. Hoyer W, Jödicke R (1995) *J Non-Cryst Solids* 192–193:102
31. Li H (2004) *J Phys Chem B* 108:5438
32. Schenk T, Simonet V, Holland-Moritz D et al (2004) *Euro Phys Lett* 65:34
33. Xie SH, Zeng XR, Qian HX (2009) *J Alloys Compd* 480:L37
34. Steenberge NV, Concstell A, Sort J et al (2008) *Mater Sci Eng A* 491:124